Applied Surface Science 527 (2020) 146818

Contents lists available at ScienceDirect

Applied Surface Science

journal homepage: www.elsevier.com/locate/apsusc

Full Length Article

Optical properties of ultrathin ZnO films fabricated by atomic layer deposition

Liping Fang[a], Haolin Li[a,b], Xuhang Ma[c], Qiuming Song[d], Rui Chen[a,*]

[a] Department of Electrical and Electronic Engineering, Southern University of Science and Technology, Shenzhen, Guangdong 518055, PR China
[b] State Key Laboratory of High Power Semiconductor Laser, School of Science, Changchun University of Science and Technology, Changchun 130022, PR China
[c] Core Research Facilities, Southern University of Science and Technology, Shenzhen, Guangdong 518055, PR China
[d] Shenzhen Institute for Quantum Science and Engineering, and Department of Physics, Southern University of Science and Technology, Shenzhen, Guangdong 518055, PR China

ARTICLE INFO

Keywords:
Ultrathin ZnO films
Optical properties
Atomic layer deposition
Spectroscopic ellipsometry
X-ray reflectivity
Quantum confinement

ABSTRACT

Ultrathin zinc oxide (ZnO) films with thickness down to several nanometers have been fabricated by atomic layer deposition. The chemical composition, surface morphology, crystalline structure, optical properties and photoluminescence characteristics of the ZnO films with various thicknesses were investigated. The X-ray photoelectric spectroscopy illustrates that the deposited films are uniformly distributed with zinc and oxygen atoms. Spectroscopic ellipsometric measurements reveal that both the refractive index and extinction coefficient decrease monotonically as the thickness of the film decreases. The thickness of the ZnO films obtained via ellipsometry is consistent with X-ray reflectivity measurements. The excitonic emission peak of the photoluminescence spectrum shifts to higher energies when the film thickness decreases to a few nanometers. This blueshift phenomenon is consistent with the expansion of the fundamental optical bandgap determined from ellipsometry, which could be well described by the effective mass model using physically meaningful parameters. The results obtained in this study could provide guidance to the design and optimization of optoelectronic devices based on ultrathin ZnO films.

1. Introduction

Zinc oxide (ZnO) is an attractive semiconductor for short wavelength optoelectronic devices due to its wide bandgap and extraordinary excitonic properties [1,2]. For bulk ZnO at room temperature, the optical bandgap is 3.3 eV and the exciton binding energy is as high as 60 meV [3]. These properties makes ZnO a promising candidate for application in, especially, low-dimensional optoelectronic devices [4] in the form of quantum dots [5,6], nanowires [7,8] and nanodiscs [9], *etc*., where novel optoelectronic properties emerge due to the quantum effects at reduced geometric size. Ultrathin ZnO film is another kind of low dimensional material with geometry reduced in the thickness direction. The optical properties, i.e. dielectric constants, optical bandgap and photoluminescence (PL), of such ZnO films might be tuned simply by the film thickness.

Since the exciton Bohr radius of ZnO is approximately 2 nm [1,2], it is of great interest to investigate the properties of ZnO films which are a few nanometers thick [10–13]. Nie *et al.* [10] found that the exciton peak of the absorption spectra of the ZnO films with thickness down to 4.8 nm follows the effective mass model derived by Brus [14], but the dielectric constants and PL properties were not studied. Mosquera *et al.* [11] investigated the dependence of the free exciton energy and core-level binding energy on the thickness of ZnO films, however, the thinnest film under study was 10 nm. Li *et al.* [12] studied the exciton binding energy and bandgap energy (determined from ellipsometry) of ZnO films with thickness down to 10 nm, the other properties were not investigated. Pal *et al.* [13] reported the bandgap enlargement of ultrathin ZnO films with only two thickness below 10 nm (5 and 9 nm), the PL properties were missing. Chaaya *et al.* [15] studied the tunable optical properties of ZnO films with thickness of 25, 50, 125 and 250 nm, which are beyond the thickness range for quantum confinement. None of the previous works have systematically studied the various properties of ultrathin ZnO films. The observed bandgap enlargement at reduced film thickness were fitted by the effective mass model with parameters which are not physically meaningful [10–13]. The quantum confinement effect has not been demonstrated convincingly. Therefore, the optical properties of ultrathin ZnO films with thickness down to a few nanometers should be investigated thoroughly.

* Corresponding author.
E-mail address: chenr@sustech.edu.cn (R. Chen).

https://doi.org/10.1016/j.apsusc.2020.146818
Received 24 March 2020; Received in revised form 27 May 2020; Accepted 27 May 2020
Available online 04 June 2020

Several methods have been used to deposit ZnO films, such as magnetron sputtering [11,12,16–23], pulsed laser deposition [10,24,25], metal–organic chemical vapor deposition [26–30] and atomic layer deposition (ALD) [15,31–38]. Among these techniques, ALD is probably the most promising approach to fabricate high quality ultrathin ZnO films with atomically specified thickness at low temperature [39–41]. Due to the merits of high conformity and accurate thickness control, ALD has been widely employed to deposit functional nanolayers for semiconductor devices [42–44], biosensors [45] and a variety of membranes in application of gas separation, water filtration and catalysis [46]. In this work, we report the optical properties of ultrathin ZnO films with thickness down to a few nanometers fabricated by ALD. The chemical composition, surface morphology, and crystalline structure of these ultrathin films were characterized thoroughly. The unique optical properties of the fabricated ultrathin ZnO films, i.e. bandgap enlargement and blueshift of PL spectra, due to quantum confinement effects were demonstrated by the effective mass model using physically meaningful parameters.

2. Material and methods

2.1. Film deposition

The ZnO films were deposited on silicon (1 0 0) substrates (Siltronix, P type, resistivity of 1–30 Ω cm) with a PicoSun R200 ALD system. The precursors were diethyl zinc (DEZ, CAS: 557–20-0, Sigma-Aldrich, 99% purity) and pure water (CAS: 7732–18-5, Sigma-Aldrich, 99.99% purity) with the chemical reaction:

$$Zn(CH_2CH_3)_2 + H_2O \rightarrow ZnO + 2C_2H_6$$

The pulse length for DEZ and pure water were 0.1 and 0.2 s, respectively. The carrier gas for the precursors was nitrogen, the flow was 150 and 200 sccm (standard cubic centimeters per minute) for DEZ and pure water, respectively. After each pulse, pure nitrogen was purged for 4 s. Before deposition, the silicon substrates were cleaned following standard RCA procedures [47]. The surface oxide was removed by dipping in buffered oxide etch solution (6:1 vol ratio of 40% ammonium fluoride in water to 49% hydrofluoric acid in water, Sigma-Aldrich, 99% purity) for 2 min. The substrate temperature was maintained at 200 °C during film deposition. After deposition, the reaction chamber was cooled down to room temperature before removing the substrate from vacuum. ZnO films with variable number of deposition cycles, i.e. 20, 30, 40, 50, 100 and 200 cycles, were deposited and the samples were named as 20C, 30C, 40C, 50C, 100C and 200C, respectively.

2.2. Film characterization

The chemical compositions of the ZnO films were characterized by X-ray photoelectron spectroscopy (XPS, Thermo Scientific ESCALAB 250Xi) measurements under ultrahigh vacuum conditions (5×10^{-8} Pa). The X-ray source was Al K_α with monochromatic emission at 1486.6 eV, and the energy resolution was 0.45 eV. Argon ions with energy of 2 keV were used to etch the ZnO films for surface contamination removal and depth profiling measurements. The surface roughness of the ZnO films was measured by an atomic force microscope (AFM, Asylum Research MFP-3D-SA) in the tapping mode. The crystalline structure of the ZnO films was characterized by an X-ray diffractometer (Rigaku SmartLab) in the θ-2θ mode. The incident angle of the Cu Kα radiation was 0.35°. The scanning angle range was 25°-75° and the step size was 0.02°. X-ray reflectivity (XRR) measurements of the ZnO films were also performed on the same diffractometer with scanning angle range of 0-6° and step size of 0.01°. The thickness and refractive index of the ZnO films were measured by a spectroscopic ellipsometer (J. A. Woollam M2000U) in the spectra range from 250 to 1000 nm, and the incident light angle was 65°. Room temperature photoluminescence (PL) of the as-deposited ZnO films were excited by a helium-cadmium (He-Cd) laser emitting at 325 nm and detected by a silicon detector.

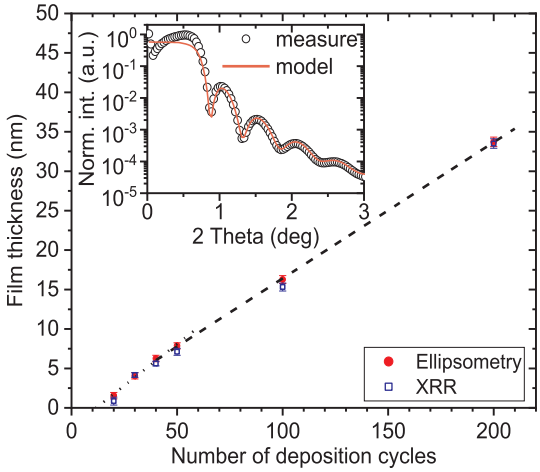

Fig. 1. Comparison of film thickness results obtained by ellipsometry and XRR. Inlet: X-ray reflectivity curve fitting result for the 100C sample.

3. Results and discussion

3.1. Deposition rate

XRR and spectroscopic ellipsometry are useful non-destructive techniques for the characterization of ultrathin films. Both of these two techniques were used to measure the ultrathin ZnO films *ex situ*. The film thickness results obtained via these two methods were compared in Fig. 1. The detailed analysis of the ellipsometry results are in the spectroscopic ellipsometry section.

It is apparently from Fig. 1 that the growth rate decreases when the film gets thicker. The growth rate drops from 0.21 ± 0.014 nm per cycle to 0.17 ± 0.002 nm per cycle when the number of ALD cycles is more than 50. Such self-limiting behavior of ultrathin ZnO films has also been observed by other researchers [32].

A typical XRR curve is shown in the inlet of Fig. 1, where the normalized X-ray reflectivity is plotted against the incident angle of X-ray. The Kiessig fringes characteristic could be clearly observed. The measured reflectivity curve is fitted by a theoretical curve simulated by the recursive Parratt's formula which includes the effect of surface and interface roughness [48]. The fitting procedure was performed by using the Rigaku GlobalFit software. Upon fitting, the film thickness, film density and surface roughness parameters could be obtained simultaneously. Good fits are obtained for all the samples, which are illustrated in Fig. S1 in the supporting information. The revealed parameters for the ultrathin ZnO films are shown in Table 1.

It is shown from Table 1 that the density of the deposited ZnO films were close to the value of bulk ZnO (5.6 g/cm^3 [49,50]), except for the 20C sample. Similar density result has been obtained by *in situ* quartz crystal microbalance measurements for ZnO films deposited by ALD

Table 1
XRR measurement results.

Sample	Thickness (nm)	Density (g/cm^3)	Roughness (nm)
20C	0.859 ± 0.501	3.45 ± 0.03	0.4070 ± 0.0050
30C	4.166 ± 0.312	5.55 ± 0.03	0.9890 ± 0.0030
40C	5.614 ± 0.302	5.56 ± 0.02	0.4317 ± 0.0020
50C	7.111 ± 0.452	5.57 ± 0.02	0.4090 ± 0.0020
100C	15.32 ± 0.502	5.56 ± 0.05	0.3744 ± 0.0016
200C	33.51 ± 0.601	5.72 ± 0.04	0.4514 ± 0.0019

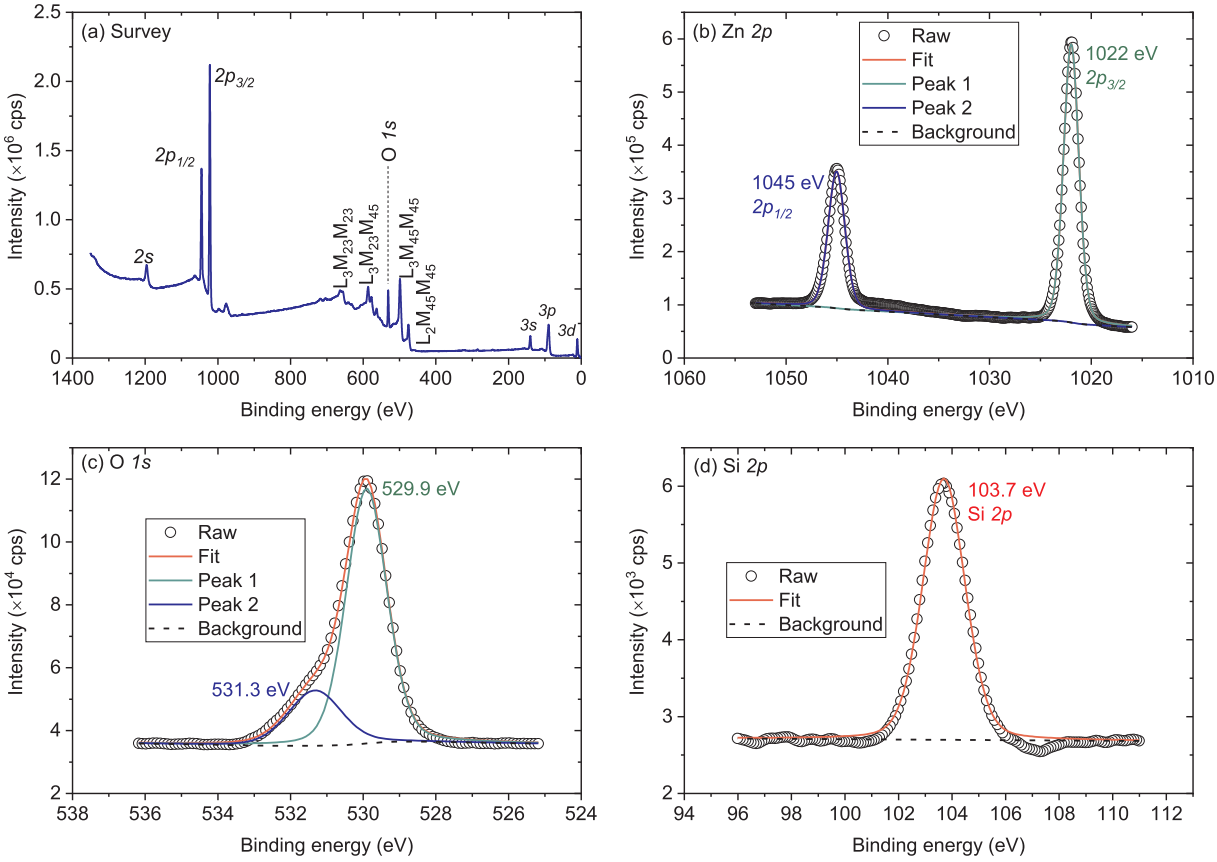

Fig. 2. (a) Survey spectrum and elemental spectra for (b) Zn 2p (c) O 1 s and (d) Si 2p for the 200C sample after Ar milling for 10 min.

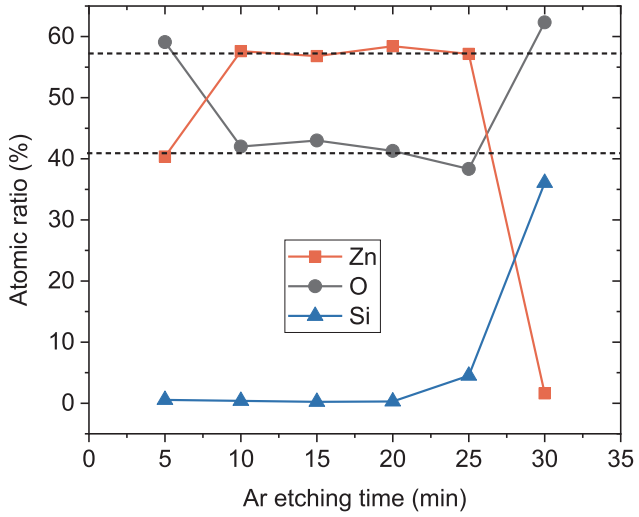

Fig. 3. Depth profiling of the 200C ZnO film sample.

[31]. In comparison, the 20C sample has a lower density, which might be due to the large density of defects, such as pores and pin holes, for film with thickness around merely one nanometer.

3.2. Chemical composition

The chemical composition of the ZnO films was characterized by XPS. The measured spectra were calibrated according to the binding energy of C *1 s* at 284.8 eV [51]. For fitting of the elemental spectra, Shirley backgrounds and Gaussian-Lorentzian type spectra were used. The typical results for the survey spectrum and the high-resolution elemental spectra are shown in Fig. 2.

As shown in Fig. 2 (a), the photoelectron and Auger lines of Zn and O are clearly observed. The high resolution spectra for Zn $2p_{1/2}$ and Zn $2p_{3/2}$ are shown in Fig. 2 (b), where both of them are fitted by single Gaussian functions. The related peak binding energies at 1045 ± 0.2 eV and 1022 ± 0.2 eV are consistent with the value shown in [51].

The O 1 s spectrum shown in Fig. 2 (c) can be decomposed into two peaks, which correspond to different chemical environments of oxygen atoms in the hexagonal wurtzite crystal of ZnO (as revealed by XRD measurements for the deposited ZnO films): the 531.3 ± 0.2 eV peak corresponds to oxygen atoms in the oxygen-deficient region, whereas the peak at 529.9 ± 0.2 eV corresponds to oxygen atom in a fully occupied crystal region. The binding energy of these two peaks are in good agreement with literature [16,52]. The Si *2p* spectrum shown in Fig. 2 (d) is fitted with a single Gaussian function with binding energy peak at 103.7 ± 0.2 eV, which corresponds to the Si-O bond [53,54].

In order to get the stoichiometric information of the deposited ZnO films, XPS depth profiling using argon ions as etchant was performed for the 200C sample. The high resolution elemental spectra of Zn, O and Si were analyzed in the fashion similar as Fig. 2. The atomic ratio of these three elements were obtained by comparing the area under the Gaussian functions weighed by the sensitivity factor for the related photoelectron line. The atomic ratio as a function of Ar etching time is plotted in Fig. 3. It is illustrated that near the top surface the oxygen atom has an atomic ratio as high as 60%, which is due to water adsorbed on the film surface. Similar analysis of the O *1 s* spectra as shown in Fig. 2 (c) would resulted in three peaks, the extra peak is related to the H-O bond, which is not shown here. After 10 min of argon ion etching, the atomic ratio becomes stable at Zn:O = 1:0.7. After 30 min etching, the signal from Zn atom disappeared. The etching rate is estimated to be 1.1 nm/min. The obtained stoichiometric value is

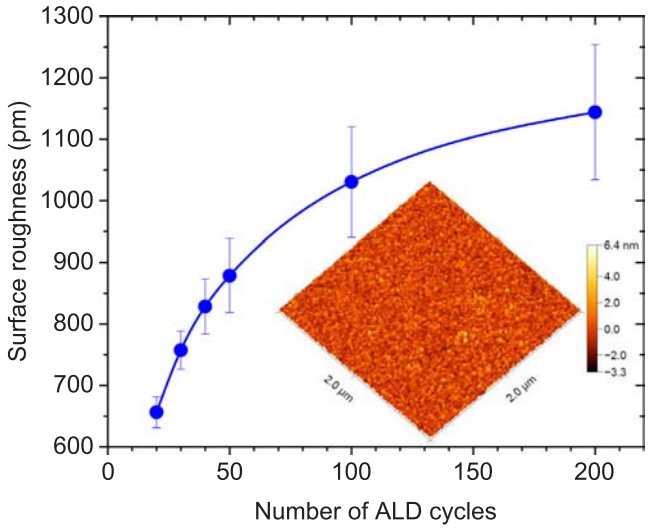

Fig. 4. Dependence of surface roughness on the number of ALD cycles. Inlet: Surface morphology of the 50C sample.

different from ZnO, which could be attributed to preferential sputtering of oxygen atoms during argon ion milling. A viable approach for more accurate determination of the film stoichiometry could be normalization of the obtained stoichiometry to that for a ZnO single crystal [55]. We will continue this interesting topic in a subsequent investigation. Nevertheless, the depth profiling results indicate that the zinc and oxygen atoms are uniformly distributed in the deposited films.

3.3. Surface morphology

The surface morphology of the ultrathin ZnO films was characterized via atomic force microscopy (AFM). A typical surface morphology is shown in the inlet of Fig. 4, based on which the root mean square surface roughness is calculated to be 0.4 nm. Similar analysis has been performed for the other samples. The dependence of surface roughness on the number of ALD cycles is shown in Fig. 4. It is depicted that the surface roughness increases monotonically as the number of the ALD cycles increases. The maximum roughness is merely around 1 nm (the 200C sample), which agrees with the surface roughness results obtained by XRR. These surface roughness results illustrate that the deposited ZnO films are flat and uniform.

3.4. Crystalline structure

The crystalline structure of the deposited ZnO films was characterized via grazing-incidence X-ray diffraction (GIXRD). The incident angle of X-ray was chosen at 0.35°, which is close to the critical angel for X-ray total-internal reflection at the ZnO-air interface. The reflection patterns for the 200C, 100C and 50C samples are shown in Fig. 5. The 40C, 30C and 20C samples show no apparent reflection peaks.

The reflection peaks were indexed using the standard inorganic crystal structure database pattern (ICSD PDF#75–0576) of hexagonal wurtzite ZnO. The diffraction results indicate that the deposited ZnO films were polycrystalline with major reflection peaks in the (1 0 0), (0 0 2) and (1 0 1) directions. Assuming the crystallites are spherical shaped, the average crystallite sizes could be estimated via Scherrer's formula [56], which is given by

$$D = 0.9\lambda/\beta cos\theta$$

where D is the average crystallite size, λ the wavelength of X-ray, β the line broadening at half the maximum intensity, and θ the Bragg angle. The estimated average crystallite size for the 200C sample is 15.9, 15.3 and 8.4 nm for the (1 0 0), (0 0 2) and (1 0 1) planes, respectively.

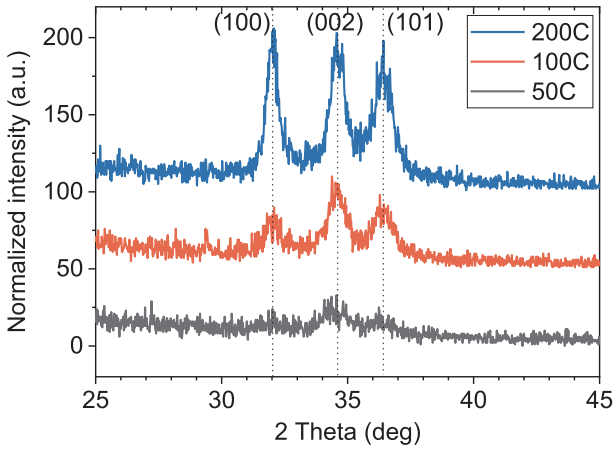

Fig. 5. GIXRD pattern of ZnO films with different thicknesses. Note that the spectra have been shifted vertically for clarity.

3.5. Spectroscopic ellipsometry

From spectroscopic ellipsometry measurements, the film thickness, refractive index and extinction coefficients of the ZnO films could be obtained simultaneously by fitting the modelled parameters to the measured ellipsometric parameters. The J. A. Woollam CompleteEASE software was used for all the fittings. The modelled ellipsometric parameters were calculated from the ZnO dispersion relation modelled by a Herzinger–Johs (HJ) Psemi-M0 parameterized oscillator function [57,58]. This oscillator function consists of four polynominals spline function connected end to end and could accurately reproduce the dielectric function of semiconductors with complicate critical point structures [20,21]. More importantly, this parametric model is Kramers–Kronig (KK) consistent and sensitive to subtle characteristics (such as the fine structure of the exciton peak), which might not be well captured by conventional physical models [59]. A comprehensive review for the conventional model dielectric functions of ZnO could be found in [60].

The nine fitting variables are the ZnO film thickness, the amplitude and energy of the UV pole, and the six parameters of the HJ PSemi-M0 model [61]: Amp (amplitude of the oscillator center energy), Br (broadening), E_0 (center energy), WR (width of right side absorption region), PR (control point position for right side), AR (control point amplitude for right side). The fitted values are shown in Table 2. All the fitting results of the ellipsometric parameters are illustrated in Fig. S2 in the supporting information. The goodness of fitting is quantified by the MSE (mean-squared-error) parameter, which is defined as the root mean squared difference between the measured and modelled functions of the ellipsometric parameters [59]. It is seen from Table 2 that the MSE value for all the samples are below 10, which indicates good fitting between the modeled and measured ellipsometric parameters. The refractive index and extinction coefficient of the ZnO films revealed by ellipsometry are plotted in Fig. 6. Generally, these two parameters increase as the number of deposition cycles increases. Note that, beyond 450 nm, the extinction coefficient for all the samples vanishes.

3.6. Photoluminescence

The luminescent properties of the deposited ultrathin ZnO films were characterized by room temperature PL. The measured spectra are shown in Fig. 7 (a). Note that the intensity is displayed on a logarithmic scale. It is depicted in Fig. 7 (a) that thicker ZnO films exhibit stronger PL intensity. Except for the 20C sample, all the other samples show the characteristic excitonic emission with peak wavelength around 380 nm (3.27 eV), which arises from high quality hexagonal wurzite ZnO [62]. The PL emission from the 20C sample was too low to be captured by the

Table 2
Ellipsometry fitting variables for the ZnO films.

Parameter	200C	100C	50C	40C	30C	20C
MSE	5.872	0.882	1.621	1.538	0.726	0.859
Thickness (nm)	33.72 ± 0.027	16.27 ± 0.007	7.86 ± 0.013	6.25 ± 0.012	4.05 ± 0.023	1.55 ± 0.013
UV Pole Amp.	4.3777	29.4497	25.9158	37.5817	9.9739	18.2591
UV Pole En.	5.911	7.508	6.526	6.656	6.144	6.544
Amp	7.239	1.347	6.928	3.682	1.808	11.554
Br	0.1196	0.111	0.225	0.2194	0.3807	0.2634
E_0	3.366	3.299	3.369	3.561	3.681	4.096
WR	22.1013	8.0836	5.7368	3.0054	12.2641	50
PR	0.993	0.00207	0.999	0.998	0.908	0.995
AR	0.236	0.00373	0.216	0.48	0.449	0.0369

detector, though there is a relatively sharp peak in the excitonic region of the optical constants shown in Fig. 6. The reason would be strong absorption by the silicon substrate and also note that the ZnO film thickness is less than 1 nm. All the samples, except for the 200C one, also show a broad green band emission, which are believed to arise from defects such as oxygen vacancies or interstitial zinc [1,2]. The 200C sample has no pronounced emission in the green band, which could be attributed to enhanced crystal quality with increased film thickness, as revealed by XRD measurements.

Furthermore, we observed the blueshift phenomenon of the excitonic PL emission as the thickness of the ZnO film decreases, as shown in Fig. 7 (b). The excitonic PL peak gradually shifts from 380 nm (3.27 eV) to 368 nm (3.37 eV) as the number of deposition cycle decreased from 200 to 30. Such blueshift phenomenon has also been observed for ZnO quantum dots with reduced diameter [5,6]. This kind of phenomenon could be attributed to the quantum confinement effects at reduced geometric size. To illustrate such an effect, we first determine the bandgap from the extinction coefficients measured by ellipsometry, and then related the blueshift of the PL spectra with the bandgap enlargement.

3.7. Optical bandgap

The absorption coefficient α of the ZnO films is calculated from the extinction coefficient k and wavelength λ by $\alpha = 4\pi k/\lambda$. For direct bandgap semiconductors such as ZnO, the absorption coefficient is related to the optical bandgap via:

$$\alpha = \frac{K(\hbar\omega - E_g)^{1/2}}{\hbar\omega}$$

where K is a constant, $\hbar\omega$ the photon energy, and E_g the bandgap. The bandgap of the ZnO film could be obtained via extrapolating of the linear region of $(\alpha\hbar\omega)^2$ vs. $\hbar\omega$ plot, which is known as Tauc's plot [19,52]. The results are shown in Fig. 8 (a).

The bandgap obtained from Fig. 8 (a) is plotted versus half of the film thickness in Fig. 8 (b). It is apparent from Fig. 8 (b) that the optical bandgap increases at reduced film thickness. We show later that such bandgap enlargement could be explained by an effective mass model. For film thickness larger than 10 nm, the bandgap plateaus approximately at 3.3 eV, which is the bandgap of bulk ZnO crystals [63]. The bandgap of spherical particle given by the effective mass model [14] is

$$E_g = E_g^{bulk} + \frac{\hbar^2\pi^2}{2R^2}\left(\frac{1}{m_e^*} + \frac{1}{m_h^*}\right) - \frac{1.8e^2}{\varepsilon R}$$

where E_g^{bulk} is the bandgap of the bulk material, $\hbar$ the reduced Planck's constant, R the radius of the particle, m_e^* the effective mass of electron, m_h^* the effective mass of hole, e the charge of an electron, and $\in$ the absolute permittivity. The second term in the effective mass model represents the bandgap enlargement due to quantum confinement, the third term represents the ground state exciton binding energy. The polarization term given by [14] is negligible, so it is not included here.

The bandgap determined from ellipsometry is compared with the effective mass model in Fig. 8 (b), which uses the following physically meaningful parameters: $E_g^{bulk} = 3.25$ eV, $m_e^* = 0.24m_0$, $m_h^* = 0.59m_0$, $\in = 3.7\in_0$ [1,2,50], where m_0 is the free electron rest mass, $\in_0$ the vacuum permittivity. For the ultrathin ZnO films in this work, the quantum confinement effect mainly lies in the thickness direction, so the particle diameter is assumed to be half of the film thickness in Fig. 8 (b). As illustrated in Fig. 8 (b), a good fit has been obtained between the measured bandgap and the effective mass model, although the effective mass model overestimates the confinement effect for particle size less than 5 nm. This phenomenon has also been noted for ZnO quantum dots [64,65].

The residual strain in the ZnO films, which mainly originates from the lattice mismatch between the substrate and the film [4,10], could also contribute to the bandgap variation [17,18,23,27]. The strain

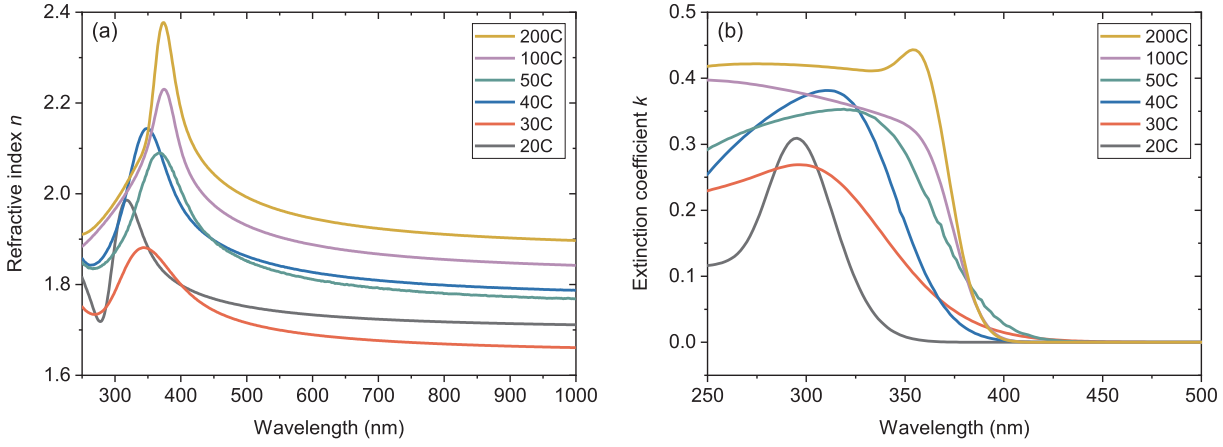

Fig. 6. (a) Refractive index and (b) extinction coefficients of the ZnO films.

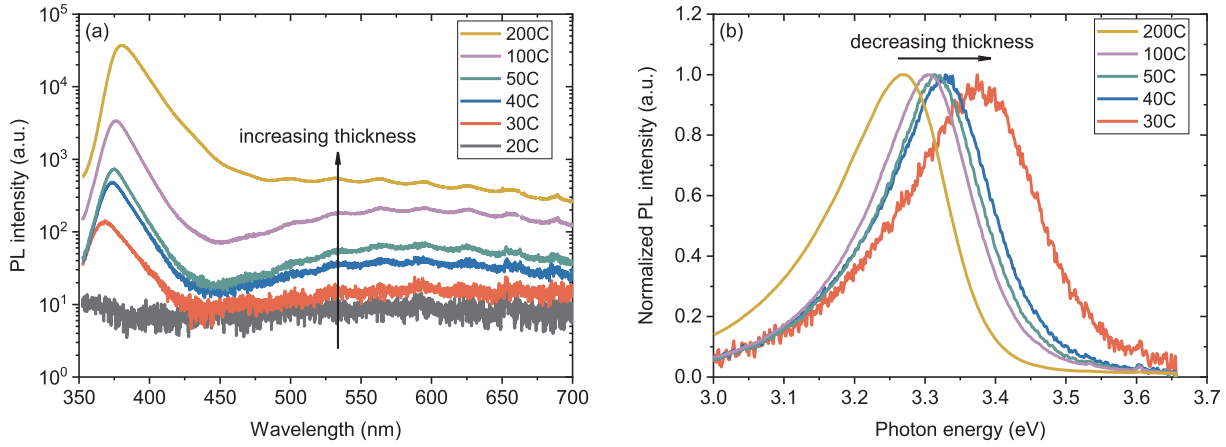

Fig. 7. (a) Room temperature PL spectra of the ZnO films and (b) normalized spectra showing the blueshift phenomenon as the film thickness decreases.

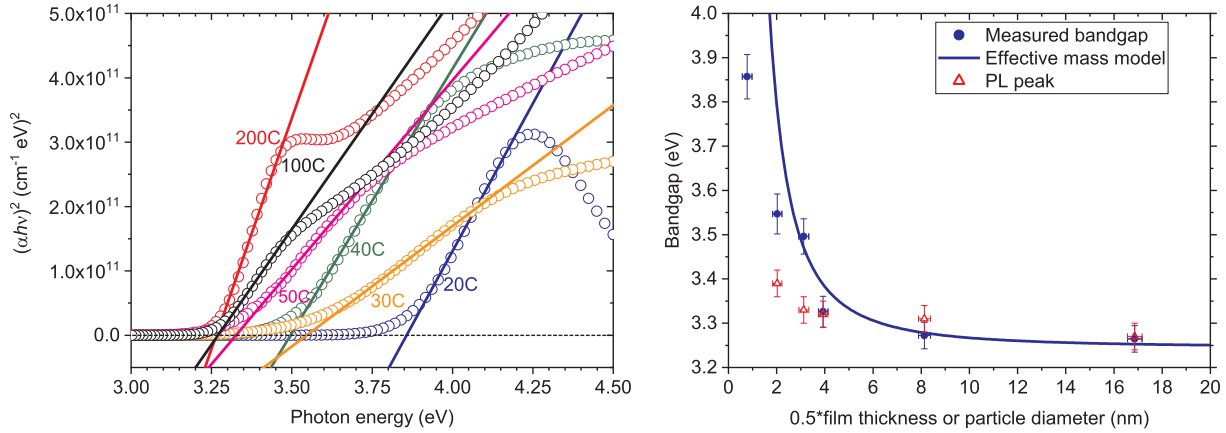

Fig. 8. (a) Tauc's plot for the ZnO films and (b) comparison of measured bandgap with effective mass model.

along the c axis of the ZnO hexagonal lattice is defined as $\varepsilon = (c - c_0)/c_0$ [17], where c is the measured lattice constant of the (0 0 2) plane and c_0 is that of an unstrained crystal. The measured lattice constant c could be estimated from the XRD diffraction peak which corresponds to the (0 0 2) reflection by the equation $c = \lambda/\sin\theta$ [22], where λ is the wavelength of X-ray, θ the Bragg angle. From the XRD patterns shown in Fig. 5, the lattice constant c is estimated to be around 5.1690 Å for the 200C, 100C, and 50C samples. If the unstrained lattice constant c_0 is taken as 5.2069 Å [50], the strain ε is estimated to be 0.7%. Ashrafi *et al.* [27] showed that below the critical thickness of 7 nm, ZnO film grew coherently, the strain level is almost constant. So the strain for the 40C, 30C and 20C might be at the same level as the 50C sample. Based on previous studies, the bandgap variation is less than 0.1 eV if the strain is less than 1% [22,23,27]. Thus the contribution of strain to the bandgap variation is limited, the main effect is quantum confinement. The PL peaks of the ZnO films have also been plotted in Fig. 8 (b). The trend of increasing of the peak photon energy qualitatively follows the trend of the bandgap enlargement. Therefore the blueshift of the PL spectra is mainly due to the quantum confinement effect when the film thickness reduces to a few nanometers.

4. Conclusion

Ultrathin zinc oxide films with thickness down to a few nanometers have been fabricated by atomic layer deposition at low temperature. The film thickness result obtained by spectroscopic ellipsometry is consistent to that by X-ray reflectivity measurements. The fabricated ultrathin films exhibit high density, approaching the density of single ZnO crystal for film thickness of merely 4 nm. The X-ray photoelectric spectroscopy results show that the deposited films are uniformly distributed with zinc and oxygen atoms. Room temperature photoluminescence emission peak of the as-deposited ZnO film shifts to larger photon energies when the thickness of the ZnO film decreases to a few nanometers. This phenomenon is consistent with the expansion of the fundamental optical bandgap of the ZnO films, which could be well explained by the effective mass model using physically meaningful parameters. The results in this work could offer guidance for the design and optimization of optoelectronic devices, such as light-emitting diodes and solar cells, which incorporate ultrathin ZnO film as functional layers.

CRediT authorship contribution statement

Liping Fang: Conceptualization, Methodology, Validation, Formal analysis, Investigation, Data curation, Writing - original draft, Writing - review & editing, Visualization, Funding acquisition. **Haolin Li:** Methodology, Validation, Formal analysis, Investigation, Data curation, Visualization, Writing - review & editing. **Xuhang Ma:** Validation, Investigation, Validation, Resources, Writing - review & editing. **Qiuming Song:** Validation, Investigation, Resources, Writing - review & editing. **Rui Chen:** Supervision, Project administration, Writing - review & editing, Funding acquisition.

Declaration of Competing Interest

The authors declare that they have no known competing financial interests or personal relationships that could have appeared to influence the work reported in this paper.

Acknowledgments

This work was supported by the National Nature Science Foundation of China (No. 61604138). ALD, XRD and AFM were performed using the tools maintained by Southern University of Science and Technology Core Research Facilities. Ellipsometry measurements were conducted at the Institute for Quantum Science and Engineering, Southern University of Science and Technology. We thank technical help from Dr. X. Gao, Dr. R. Li, Mr. J. Yu and Mr. X. Zhang.

Appendix A. Supplementary data

Supplementary data to this article can be found online at https://doi.org/10.1016/j.apsusc.2020.146818.

References

[1] C. Jagadish, S.J. Pearton (Eds.), Zinc Oxide Bulk, Thin Films and Nanostructures: Processing, Properties, and Applications, Elsevier, 2006.
[2] H. Morkoç, Ü. Özgür, Zinc Oxide: Fundamentals, John Wiley & Sons, Materials and Device Technology, 2008.
[3] A. Janotti, C.G. Van de Walle, Fundamentals of zinc oxide as a semiconductor, Rep. Prog. Phys. 72 (12) (2009) 126501.
[4] Ü. Özgür, Y.I. Alivov, C. Liu, A. Teke, M.A. Reshchikov, S. Doğan, V. Avrutin, S.J. Cho, H. Morkoç, A comprehensive review of ZnO materials and devices, J. Appl. Phys. 98 (4) (2005) 041301.
[5] K.F. Lin, H.M. Cheng, H.C. Hsu, L.J. Lin, W.F. Hsieh, Band gap variation of size-controlled ZnO quantum dots synthesized by sol–gel method, Chem. Phys. Lett. 409 (4) (2005) 208–211.
[6] H.M. Cheng, K.F. Lin, H.C. Hsu, W.F. Hsieh, Size dependence of photoluminescence and resonant Raman scattering from ZnO quantum dots, Appl. Phys. Lett. 88 (26) (2006) 261909.
[7] R. Chen, Q.L. Ye, T.C. He, T. Wu, H.D. Sun, Uniaxial tensile strain and exciton-phonon coupling in bent ZnO nanowires, Appl. Phys. Lett. 98 (24) (2011) 241916.
[8] R. Chen, Q.L. Ye, T. He, V.D. Ta, Y. Ying, Y.Y. Tay, T. Wu, H. Sun, Exciton localization and optical properties improvement in nanocrystal-embedded ZnO core-shell nanowires, Nano Lett. 13 (2) (2013) 734–739.
[9] R. Chen, B. Ling, X.W. Sun, H.D. Sun, Room temperature excitonic whispering gallery mode lasing from high-quality hexagonal ZnO microdisks, Adv. Mater. 23 (19) (2011) 2199–2204.
[10] J.C. Nie, J.Y. Yang, Y. Piao, H. Li, Y. Sun, Q.M. Xue, C.M. Xiong, R.F. Dou, Q.Y. Tu, Quantum confinement effect in ZnO thin films grown by pulsed laser deposition, Appl. Phys. Lett. 93 (17) (2008) 173104.
[11] A.A. Mosquera, D. Horwat, A. Rashkovskiy, A. Kovalev, P. Miska, D. Wainstein, J.M. Albella, J.L. Endrino, Exciton and core-level electron confinement effects in transparent ZnO thin films, Sci. Rep. 3 (1) (2013) 1714.
[12] X.D. Li, T.P. Chen, P. Liu, Y. Liu, Z. Liu, K.C. Leong, A study on the evolution of dielectric function of ZnO thin films with decreasing film thickness, J. Appl. Phys. 115 (10) (2014) 103512.
[13] D. Pal, J. Singhal, A. Mathur, A. Singh, S. Dutta, S. Zollner, S. Chattopadhyay, Effect of substrates and thickness on optical properties in atomic layer deposition grown ZnO thin films, Appl. Surf. Sci. 421 (2017) 341–348.
[14] L.E. Brus, Electron-electron and electron-hole interactions in small semiconductor crystallites: The size dependence of the lowest excited electronic state, J. Chem. Phys. 80 (9) (1984) 4403–4409.
[15] A. Abou Chaaya, R. Viter, M. Bechelany, Z. Alute, D. Erts, A. Zalesskaya, K. Kovalevskis, V. Rouessac, V. Smyntyna, P. Miele, Evolution of microstructure and related optical properties of ZnO grown by atomic layer deposition, Beilstein J Nanotechnol 4 (2013) 690–698.
[16] M. Chen, X. Wang, Y.H. Yu, Z.L. Pei, X.D. Bai, C. Sun, R.F. Huang, L.S. Wen, X-ray photoelectron spectroscopy and auger electron spectroscopy studies of Al-doped ZnO films, Appl. Surf. Sci. 158 (1) (2000) 134–140.
[17] R. Hong, J. Huang, H. He, Z. Fan, J. Shao, Influence of different post-treatments on the structure and optical properties of zinc oxide thin films, Appl. Surf. Sci. 242 (3) (2005) 346–352.
[18] B.C. Mohanty, Y.H. Jo, D.H. Yeon, I.J. Choi, Y.S. Cho, Stress-induced anomalous shift of optical band gap in ZnO: Al thin films, Appl. Phys. Lett. 95 (6) (2009) 062103.
[19] P. Mondal, D. Das, Transparent and conducting intrinsic ZnO thin films prepared at high growth-rate with c-axis orientation and pyramidal surface texture, Appl. Surf. Sci. 286 (2013) 397–404.
[20] J.M. Khoshman, J.N. Hilfiker, N. Tabet, M.E. Kordesch, Multiple oscillator models for the optical constants of polycrystalline zinc oxide thin films over a wide wavelength range, Appl. Surf. Sci. 307 (2014) 558–565.
[21] E. Mammadov, N. Naghavi, Z. Jehl, G. Renou, T. Tiwald, N. Mamedov, D. Lincot, J.F. Guillemoles, Dielectric function of zinc oxide thin films in a broad spectral range, Thin Solid Films 571 (2014) 593–596.
[22] Y. Wang, W. Tang, J. Liu, L. Zhang, Stress-induced anomalous shift of optical band gap in Ga-doped ZnO thin films: Experimental and first-principles study, Appl. Phys. Lett. 106 (2015).
[23] H.J. Choi, W. Jang, B.C. Mohanty, Y.S. Jung, A. Soon, Y.S. Cho, Origin of prestress-driven optical modulations of flexible ZnO thin films processed in stretching mode, J. Phys. Chem. Lett. 9 (20) (2018) 5934–5939.
[24] X.W. Sun, H.S. Kwok, Optical properties of epitaxially grown zinc oxide films on sapphire by pulsed laser deposition, J. Appl. Phys. 86 (1) (1999) 408–411.
[25] F. Tumino, C.S. Casari, M. Passoni, C.E. Bottani, A.L. Bassi, Pulsed laser deposition of two-dimensional ZnO nanocrystals on Au(111): growth, surface structure and electronic properties, Nanotechnology 27 (47) (2016) 475703.
[26] S.W. Kim, S. Fujita, S. Fujita, Self-organized ZnO quantum dots on SiO2/Si substrates by metalorganic chemical vapor deposition, Appl. Phys. Lett. 81 (26) (2002) 5036–5038.
[27] A.B.M.A. Ashrafi, N.T. Binh, B. Zhang, Y. Segawa, Strain relaxation and its effect in exciton resonance energies of epitaxial ZnO layers grown on 6H-SiC substrates, Appl. Phys. Lett. 84 (15) (2004) 2814–2816.
[28] S.T. Tan, B.J. Chen, X.W. Sun, W.J. Fan, H.S. Kwok, X.H. Zhang, S.J. Chua, Blueshift of optical band gap in ZnO thin films grown by metal-organic chemical-vapor deposition, J. Appl. Phys. 98 (1) (2005) 013505.
[29] M.E. Fragala, G. Malandrino, M.M. Giangregorio, M. Losurdo, G. Bruno, S. Lettieri, L.S. Amato, P. Maddalena, Structural, optical, and electrical characterization of ZnO and Al-doped ZnO thin films deposited by MOCVD, Chem. Vap. Deposition 15 (2009) 327–333.
[30] J. Jiang, L. Zhu, Y. Wu, Y. Zeng, H. He, J. Lin, Z. Ye, Effects of phosphorus doping in ZnO nanocrystals by metal organic chemical vapor deposition, Mater. Lett. 68 (2012) 258–260.
[31] J.W. Elam, S.M. George, Growth of ZnO/Al_2O_3 alloy films using atomic layer deposition techniques, Chem. Mater. 15 (4) (2003) 1020–1028.
[32] D.D. Fong, J.A. Eastman, S.K. Kim, T.T. Fister, M.J. Highland, P.M. Baldo, P.H. Fuoss, In situ synchrotron x-ray characterization of ZnO atomic layer deposition, Appl. Phys. Lett. 97 (19) (2010) 191904.
[33] Y.C. Cheng, K.Y. Yuan, M.J. Chen, ZnO thin films prepared by atomic layer deposition at various temperatures from 100 to 180 °C with three-pulsed precursors in every growth cycle, J. Alloys Compd. 685 (2016) 391–394.
[34] B. Macco, H.C.M. Knoops, M.A. Verheijen, W. Beyer, M. Creatore, W.M.M. Kessels, Atomic layer deposition of high-mobility hydrogen-doped zinc oxide, Sol. Energy Mater. Sol. Cells 173 (2017) 111–119.
[35] S. Kim, S. Lee, S.-Y. Ham, D.-H. Ko, S. Shin, Z. Jin, Y.-S. Min, A kinetic study of ZnO atomic layer deposition: Effects of surface hydroxyl concentration and steric hindrance, Appl. Surf. Sci. 469 (2019) 804–810.
[36] A.A. Chaaya, R. Viter, I. Baleviciute, M. Bechelany, A. Ramanavicius, Z. Gertnere, D. Erts, V. Smyntyna, P. Miele, Tuning optical properties of Al_2O_3/ZnO nanolaminates synthesized by atomic layer deposition, J. Phys. Chem. C 118 (7) (2014) 3811–3819.
[37] M. Baitimirova, R. Viter, J. Andzane, A. van der Lee, D. Voiry, I. Iatsunskyi, E. Coy, L. Mikoliunaite, S. Tumenas, K. Załęski, Z. Balevicius, I. Baleviciute, A. Ramanaviciene, A. Ramanavicius, S. Jurga, D. Erts, M. Bechelany, Tuning of structural and optical properties of graphene/ZnO nanolaminates, J. Phys. Chem. C 120 (41) (2016) 23716–23725.
[38] R. Viter, I. Iatsunskyi, V. Fedorenko, S. Tumenas, Z. Balevicius, A. Ramanavicius, S. Balme, M. Kempiński, G. Nowaczyk, S. Jurga, M. Bechelany, Enhancement of electronic and optical properties of ZnO/Al_2O_3 nanolaminate coated electrospun nanofibers, J. Phys. Chem. C 120 (9) (2016) 5124–5132.
[39] S.M. George, Atomic layer deposition: An overview, Chem. Rev. 110 (1) (2010) 111–131.
[40] V. Miikkulainen, M. Leskelä, M. Ritala, R.L. Puurunen, Crystallinity of inorganic films grown by atomic layer deposition: Overview and general trends, J. Appl. Phys. 113 (2) (2013) 021301.
[41] R.W. Johnson, A. Hultqvist, S.F. Bent, A brief review of atomic layer deposition: from fundamentals to applications, Mater. Today 17 (5) (2014) 236–246.
[42] M. Mattinen, G. Popov, M. Vehkamäki, P.J. King, K. Mizohata, P. Jalkanen, J. Räisänen, M. Leskelä, M. Ritala, Atomic layer deposition of emerging 2D semiconductors, HfS_2 and ZrS_2, for optoelectronics, Chem. Mater. 31 (15) (2019) 5713–5724.
[43] R.A. Ovanesyan, E.A. Filatova, S.D. Elliott, D.M. Hausmann, D.C. Smith, S. Agarwal, Atomic layer deposition of silicon-based dielectrics for semiconductor manufacturing: Current status and future outlook, J. Vac. Sci. Technol., A 37 (2019) (6).
[44] S.-J. Ding, X. Wu, Superior atomic layer deposition technology for amorphous oxide semiconductor thin-film transistor memory devices, Chem. Mater. 32 (4) (2020) 1343–1357.
[45] O. Graniel, M. Weber, S. Balme, P. Miele, M. Bechelany, Atomic layer deposition for biosensing applications, Biosens. Bioelectron. 122 (2018) 147–159.
[46] M. Weber, A. Julbe, A. Ayral, P. Miele, M. Bechelany, Atomic layer deposition for membranes: Basics, challenges, and opportunities, Chem. Mater. 30 (21) (2018) 7368–7390.
[47] K. Reinhardt, W. Kern, Handbook of Silicon Wafer Cleaning, Technology, William Andrew, 2018.
[48] A. Gibaud, M.S. Chebil, T. Beuvier, X-Ray Reflectivity, in: G. Bracco, B. Holst (Eds.), Surface Science Techniques, Springer, Berlin Heidelberg, Berlin, Heidelberg, 2013, pp. 191–216.
[49] D.R. Lide, CRC Handbook of Chemistry and Physics, CRC Press, 2004.
[50] D.P. Norton, Y.W. Heo, M.P. Ivill, K. Ip, S.J. Pearton, M.F. Chisholm, T. Steiner, ZnO: growth, doping & processing, Mater. Today 7 (6) (2004) 34–40.
[51] J.F. Moulder, W.F. Stickle, P.E. Sobol, K.D. Bomben, Handbook of X-ray Photoelectron Spectroscopy, Physical Electronics Inc, Eden Prairie, Minnesota, 1995.
[52] V. Kumar, H.C. Swart, O.M. Ntwaeaborwa, R.E. Kroon, J.J. Terblans, S.K.K. Shaat, A. Yousif, M.M. Duvenhage, Origin of the red emission in zinc oxide

nanophosphors, Mater. Lett. 101 (2013) 57–60.
[53] Q. Huang, M. Liu, J. Zhao, J. Chen, G. Zeng, H. Huang, J. Tian, Y. Wen, X. Zhang, Y. Wei, Facile preparation of polyethylenimine-tannins coated SiO_2 hybrid materials for Cu^{2+} removal, Appl. Surf. Sci. 427 (2018) 535–544.
[54] Y.C. Tsai, J. Shieh, Growing invisible silica nanowires on fused silica plates provides highly transparent and superwetting substrates, Appl. Surf. Sci. 479 (2019) 619–625.
[55] E. Guziewicz, M. Godlewski, L. Wachnicki, T.A. Krajewski, G. Luka, S. Gieraltowska, R. Jakiela, A. Stonert, W. Lisowski, M. Krawczyk, J.W. Sobczak, A. Jablonski, ALD grown zinc oxide with controllable electrical properties, Semicond. Sci. Technol. 27 (7) (2012) 074011.
[56] A.L. Patterson, The Scherrer formula for X-ray particle size determination, Phys. Rev. 56 (10) (1939) 978–982.
[57] C.M. Herzinger, B.D. Johs, Dielectric function parametric model, and method of use, in, US Patents, US, 1998.
[58] B. Johs, J.A. Woollam, C.M. Herzinger, J.N. Hilfiker, R.A. Synowicki, C.L. Bungay, Overview of variable-angle spectroscopic ellipsometry (VASE): II, SPIE, Advanced applications, 1999.
[59] H. Fujiwara, Spectroscopic Ellipsometry: Principles and Applications, Wiley, Tokyo, 2007.
[60] A.B. Djurišić, Y. Chan, E. Herbert, Li, Progress in the room-temperature optical functions of semiconductors, Mater. Sci. Eng., R 38 (6) (2002) 237–293.
[61] J.A. Wollam Co., Guide to Using WVASE32: Spectroscopic Ellipsometry Data Acquisition and Analysis Software, 2008.
[62] G.H. Lee, T. Kawazoe, M. Ohtsu, Difference in optical bandgap between zinc-blende and wurtzite ZnO structure formed on sapphire (0001) substrate, Solid State Commun. 124 (5) (2002) 163–165.
[63] V. Srikant, D.R. Clarke, On the optical band gap of zinc oxide, J. Appl. Phys. 83 (10) (1998) 5447–5451.
[64] T.J. Jacobsson, T. Edvinsson, Absorption and fluorescence spectroscopy of growing ZnO quantum dots: Size and band gap correlation and evidence of mobile trap states, lnorg, Chem. 50 (19) (2011) 9578–9586.
[65] R. Viswanatha, S. Sapra, B. Satpati, P.V. Satyam, B.N. Dev, D.D. Sarma, Understanding the quantum size effects in ZnO nanocrystals, J. Mater. Chem. 14 (4) (2004) 661–668.